

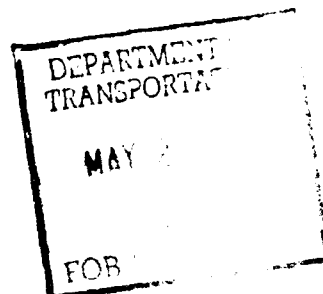
DOT/FAA/NR-91/3

Program Director
for Surveillance
Washington, D.C. 20591

AD-A236 110



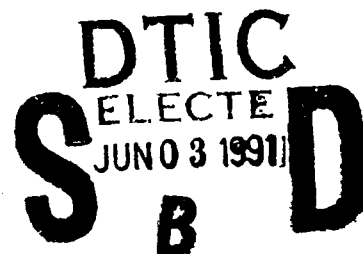
Enhancements to the Terminal
Doppler Weather Radar
Gust Front Algorithm



National Severe Storms Laboratory
1313 Halley Circle
Norman, Oklahoma 73069

December 1990

Interim Report



This document is available to the public
through the National Technical Information
Service, Springfield, Virginia 22161.

DISTRIBUTION STATEMENT A

Approved for public release;
Distribution Unlimited

*Original contains color
plates. All DTIC reproductions
will be in black and
white.



U.S. Department of Transportation
Federal Aviation Administration

91-00881



91 5 30 051

Notice

This document is disseminated under the sponsorship of the U.S. Department of Transportation in the interest of information exchange. The U.S. Government assumes no liability for the contents or use thereof.

1. Report No. DOT/FAA/NR-91/3	2. Government Accession No.	3. Recipient's Catalog No.	
4. Title and Subtitle "ENHANCEMENTS TO THE TDWR GUST FRONT ALGORITHM"		5. Report Date December 1990	
		6. Performing Organization Code MGG000	
		8. Performing Organization Report No.	
7. Author(s) Laurie G. Hermes, Kevin W. Thomas, Gregory J. Stumpf and Michael D. Eilts		10. Work Unit No. (TRAIS)	
9. Performing Organization Name and Address National Severe Storms Laboratory 1313 Halley Circle Norman, Oklahoma 73069		11. Contract or Grant No. DTFA01-80-Y-10524	
		13. Type of Report and Period Covered INTERIM REPORT	
12. Sponsoring Agency Name and Address U.S. Department of Transportation Federal Aviation Administration Program Director for Surveillance Washington, D.C. 20591		14. Sponsoring Agency Code ANR-150	
15. Supplementary Notes			
16. Abstract <p>During the 1988 Operational Test and Evaluation of the FAA's Terminal Doppler Weather Radar System (TDWR), a real-time test of the gust front algorithm capabilities in a High Plains environment (Denver, CO) was accomplished. Further evaluation of the algorithm's detection capability in the Great Plains (Kansas City, KS) was conducted in 1989. Based on these operations and additional post-analysis, deficiencies in several techniques used by the TDWR gust front algorithm were noted. As a result, modifications such as feature error checking and feature checking prior to polynomial fitting were included in the algorithm. Improvements to the techniques used to vertically associate features, determine gust front orientations, and to produce gust front representations and forecasts have also been implemented. False algorithm detections, specifically those caused by the detection of radial convergence associated with the low-level jet phenomenon, are discussed.</p>			
17. Key Words algorithm, Doppler radar, gust front low-level jet, forecasting		18. Distribution Statement This document is available to the public through the National Technical Information Service, Springfield, Virginia 22161.	
19. Security Classif. (of this report) Unclassified	20. Security Classif. (of this page) Unclassified	21. No. of Pages 64	22. Price

PREFACE

Editing of the manuscript was greatly assisted by the talents of Drs. Edward Brandes, Dusan Zrnić, and Richard Doviak, and Mr. Arthur Witt of NSSL. Figures were expertly drafted by Joan Kimpel. George Thomas Megehee (formerly of CIMMS) provided the analysis and figures for Section 8. Sonia Lasher (1989 summer student at NSSL from Saint Louis University) provided analysis and figures for Section 10. Mike Jain of NSSL deserves much credit for providing a stable computing environment for algorithm developments. Thanks also go to the MIT Lincoln Laboratory FL-2 site personnel and Group 40 for data acquisition, initial post-processing, and software tools. Data used in this report were provided by MIT Lincoln Laboratory under sponsorship from the Federal Aviation Administration.

TABLE OF CONTENTS

Abstract	i
Preface	ii
List of Figures	iv
List of Tables	vii
Acronyms	viii
1. Introduction	1
2. Background and Terminology	3
3. Algorithm Modifications	5
3.A. Feature Error Checking	5
3.B. Vertical Association	8
3.C. Detection of Fronts Tracking Over the Radar Site	13
3.D. Gust Front Orientation	18
3.E. Feature Checking Prior to Polynomial Fitting	21
3.F. Depiction of Long Gust Fronts	26
3.G. Gust Front Forecasting	26
4. False Algorithm Detections Caused by Low-level Jets	32
5. False Alarm and Wind Estimate Investigations	40
6. Conclusions	41
7. References	44
Appendix A. Algorithm Performance Statistics	45
Appendix B. Enhanced Algorithm Outline	49



Accession For	
NTIS GRA&I	<input checked="" type="checkbox"/>
DTIC TAB	<input type="checkbox"/>
Unannounced	<input type="checkbox"/>
Justification	
By	
Distribution/	
Availability Codes	
Dist	Avail and/or Special
A-1	

LIST OF FIGURES

- Figure 1. An example of a feature (dashed green) that includes shear segments from the same azimuth. The dashed lines connect the peak shear locations of the individual shear segments. The secondary radially convergent area is highlighted in yellow. The algorithm detection (bold red curve) is improperly positioned in a divergent area.
- Figure 2. The feature from Figure 1, now two features, after the error checking procedure. Note that the new gust front detection (bold curve) more closely matches the convergent area furthest in range. The secondary convergent area did not pass the front length threshold of 10 km.
- Figure 3. Lower scan features are represented by dashed lines and have dashed vertical continuity boxes. Upper scan features are represented by solid lines and have solid vertical continuity boxes. Feature centroids are represented by (.).
- Figure 4. Four features that form a candidate gust front detection. Dashed lines represent features on the lower scan while solid lines represent features on the upper scan. Association is accomplished using the end point comparison technique.
- Figure 5. Detection of a curved gust front (bold red curve) produced by vertical association using end point comparisons. These features were previously unassociated using the vertical continuity box (Figure 3). Dashed lines represent features on the lower scan. Solid lines represent features on the upper scan.
- Figure 6. An example of reduced algorithm detection capability for a front with uniform velocity difference (10 m s^{-1} and length (50 km) approaching the radar. The solid curve indicates convergence areas where velocity difference is greater than or equal 5 m s^{-1} . Hatched area indicate a velocity difference of less than 5 m s^{-1} .
- Figure 7. Gust front detections (a-e) for 5 of 9 volume scans at ten minute intervals. The thin cyan curve indicates the detection without the overhead tracking technique. The bold red curve is the detection produced using overhead tracking.

- Figure 7. (continued) Gust front detections (f-i) for 4 of 9 volume scans at ten minute intervals. The thin cyan curve is the detection without the overhead tracking technique. The bold red curve is the detection produced using overhead tracking.
- Figure 8. Example of gust front detection (bold curve) when front orientation is set to the orientation of the longest feature prior to polynomial fitting. The hatched region defines a subset of y values that have similar values of x. Dashed lines indicate features from the lower elevation scan. Solid lines indicate features from the upper elevation scan.
- Figure 9a. The dashed lines represent features from the low elevation scan and the solid lines represent features from the upper elevation scan. The bold line is the resultant detection after polynomial fitting. "Hook" region is highlighted in yellow.
- Figure 9b. The dashed lines represent features from the low elevation scan and the solid lines represent features from the upper elevation scan. The bold line is the resultant detection after polynomial fitting. "Split" region is highlighted in yellow.
- Figure 10. Example peak shear locations (.) for a front that undergoes point removal by the technique described in this section. Points within Areas A1, A2, and C are removed. Points within Area B remain. The x-axis is parallel to the front orientation. Range rings and north arrow show the radar coordinate system for reference.
- Figure 11a. The front detection after the removal of the hook feature points from the example given in Figure 9a.
- Figure 11b. The front detection after the removal of the split feature points from the example given in Figure 9b.
- Figure 12. Results from the wiggle fixing procedure. The red curve is an example of a merged third and fifth order polynomial fit. The magenta curve is an example of the original fifth order fit. Square (■) and plus (+) symbols are the peak shear locations of the vertically associated features.
- Figure 13. Example of two fronts associated in time (t_0 is the current scan, t_{-1} is the previous scan), for which the forecasting procedure will not produce forecasts.

- Figure 14. Two examples of 10 minute algorithm forecasts (solid curve), a) using the centroid-to-centroid technique, and b) using the "expansion" technique. The verification front (hatched curve) is provided for reference.
- Figure 15. A Doppler velocity pattern produced by a simple model of the jet phenomenon. wind direction is uniform with height. Maximum horizontal wind speed is 20 m s^{-1} .
- Figure 16. Radar velocity display for May 4, 1989, 0619 UTC from the FL-2 radar's 1.0° elevation scan. The curve is the low level jet detection by the algorithm.
- Figure 17. Distribution of average peak shear ($\text{m s}^{-1} \text{ km}^{-1}$) for a) low-level jet detections and b) gust front detections.
- Figure 18. Distribution of average velocity difference (m s^{-1}) for a) low-level jet detections and b) gust front detections.
- Figure 19. Wind speed versus height for 04 May 1989 low-level jet, for a) 0605 UTC, b) 0621 UTC, and c) 0642 UTC. No surface wind observation was available on this date.
- Figure 20. Wind direction versus height for 04 May 1989 low-level jet, for a) 0605 UTC, b) 0621 UTC, and c) 0642 UTC. No surface wind observation was available on this date.

LIST OF TABLES

- Table. 1 Percentage of Gust Front Detections Modified using the End Point Comparison Technique Rather than the Vertical Continuity Box
- Table 2. Distribution of Distances Between Verification Fronts and Forecasts Produce by the Centroid-to-Centroid and Expansion Techniques
- Table 3. Means and Standard Deviations of Average Peak Shear ($\text{m s}^{-1} \text{ km}^{-1}$) and Average Velocity Difference (m s^{-1}) from 41 Gust Fronts and 17 Low-level Jet Detections

Acronyms

ATC -	Air Traffic Control
FAA -	Federal Aviation Administration
FAR -	False alarm ratio or probability of false detection
FL-2 -	10 cm Doppler radar operated by MIT/LL
LL -	Lincoln Laboratory
MIT -	Massachusetts Institute of Technology
NCAR -	National Center for Atmospheric Research
NSSL -	National Severe Storms Laboratory
OT&E -	Operational Test and Evaluation
POD -	Probability of Detection
SNR -	Signal-to-Noise Ratio
TDWR -	Terminal Doppler Weather Radar
TRACON -	Terminal Radar Approach Control
VAD -	Velocity Azimuth Display

1. Introduction

In the mid-1980's, development and testing of a gust front detection algorithm began at the National Severe Storms Laboratory (NSSL) (Uyeda and Zrnić, 1985,1986). Since that time, several upgrades to the procedures and techniques which the algorithm uses to detect and forecast gust fronts have been made (Witt and Smith, 1987; Witt et al., 1989; Smith et al., 1989). Most of these upgrades were based on observations made in Denver, CO during the Summer of 1987 and were subsequently tested during the Operational Test and Evaluation (OT&E) of the Federal Aviation Administration's (FAA) Terminal Doppler Weather Radar (TDWR) system (Turnbull et al., 1989). During the OT&E, the gust front detection products, along with other outputs from the TDWR system, were used at the Stapleton International Airport in Denver, CO to provide real-time wind shear hazard warnings for arriving and departing aircraft. Gust front detection and wind shift products were also used by air traffic management (Air Traffic Control (ATC) and Terminal Radar Approach Control (TRACON)) to help plan for runway changes and to establish acceptance rates for airport traffic.

The 1988 OT&E also provided for an evaluation of gust front algorithm's capability to detect significant gust fronts in the High Plains (Denver, CO). Further evaluation of the algorithm's detection capability in the Great Plains (Kansas City, KS) was conducted from May through August of 1989. Both tests used data from the Massachusetts Institute of Technology/Lincoln Laboratory (MIT/LL) FL-2 radar.

As a result of these operations, comments regarding algorithm performance were received from personnel of the National Center for Atmospheric Research (NCAR), the FAA Technical Center and Transportation Systems Center (TSC), MIT/LL Air Traffic Surveillance group, and Air Traffic Control (ATC) of both the Stapleton and Kansas City International airports. Further evaluation of the algorithm was provided by the post-analysis statistics compiled by Klinge-Wilson et al. (1989). Meteorologists from NSSL and the FL-2 site personnel monitored algorithm performance during the real-time operations.

Based on these activities and additional post-analysis, the following improvements to the gust front algorithm have been suggested: 1) update the algorithm products (detections and forecasts) more frequently (one minute versus five minute update rate), 2) detect microburst-induced gust fronts that are shorter than the algorithm length threshold of 10 km, 3) reduce the frequency of intermittent detections and forecasts for gust fronts of moderate or weak intensity, 4) increase the percentage of gust front length detected, 5) eliminate the dependence on centroid location from the forecasting technique, 6) investigate false detections and determine their sources, and 7) investigate the source of occasionally unrepresentative wind estimates.

This report summarizes the modifications made to correct some of the deficiencies of the algorithm. A description of how each modification corrects or helps eliminate a known deficiency and

statistics comparing before and after algorithm performance are also given. Section 10 recounts the false detections by the algorithm associated with the low-level jet phenomenon prevalent across the Great Plains. Appendix A furnishes a preliminary indication of the performance of the enhanced algorithm. Appendix B summarizes the performance of the 1988 OT&E version of the algorithm for the same data base. Appendix C is a detailed outline of algorithm procedures and techniques.

2. Background and Terminology

A gust front is the region of rapid wind increase or shear at the leading edge of the cold air outflow from a thunderstorm. The algorithm relies on the identification of the main attribute which gust fronts possess in Doppler velocity fields, i.e., regions of radial convergence. Using data smoothed with a running average (across a radial distance of approximately 1 km), the algorithm searches along a radial for **shear segments**, runs of decreasing Doppler velocity (radial convergence). Several attributes of shear segments that will be referenced in this report include: 1) the **velocity difference** between the beginning and ending radial velocities of the shear segment, 2) the maximum velocity difference computed over a distance of ~ 1 km within the shear segment (referred to as **peak shear**), and 3) the slant range to the center of peak shear, i.e., **peak shear location**. To allow for a high Probability of Detection (POD) of gust fronts with moderate

intensity (velocity difference across the boundary of $> 10 \text{ m s}^{-1}$) for TDWR operations, the minimum velocity difference threshold saving shear segments is set at 5 m s^{-1} for both the lower and upper elevation scan. The peak shear threshold is the same for both scans, $2 \text{ m s}^{-1} \text{ km}^{-1}$.

Individual shear segments are combined into **features** based on spatial proximity (**feature building**). Witt and Smith (1987) sort shear segments into a common feature if their peak shear locations are near in azimuth and range. Adaptable thresholds for feature building are a maximum azimuthal separation of 3.3° and maximum range separation of 2 km. Features comprised of fewer than five segments or having lengths (the distance between end points of the feature) less than a threshold (4 km) are discarded. Two features from the same elevation scan are combined if the end points of the features are within a specified distance (5 km).

Next, features from the two elevation scans are **vertically associated** to form gust front detections. The peak shear locations of the detection are smoothed using the method of least-squares in the x, y Cartesian coordinate system. A fifth-order (third-order) polynomial is used for the **gust front representation** when the front length is greater than 20 km (less than or equal to 20 km). Front detections are **time associated** when the distance between the centroids of fronts from the current volume scan and previous volume scan pass a threshold ($\approx 10 \text{ km}$). After which, the **forecasting** of gust fronts and the computation of **horizontal wind estimates** ahead and behind the gust front are possible.

3. Algorithm Modifications

Several performance enhancements were added to the gust front algorithm prior to the 1988 TDWR OT&E. As a result of this operational evaluation, several of these enhancements and other techniques that the algorithm uses to produce features, associate features, and represent and forecast gust fronts were assessed for the purpose of improving POD, eliminating false detections, and improving the percentage of total gust front length that the algorithm detects. The following sections discuss the most significant of these algorithm modifications as well as their impact on algorithm performance.

3.A. Feature Error Checking

The purpose of feature error checking is to: 1) remove shear segments and shear features induced by ground clutter, 2) provide for a better gust front representation by reducing the variance of the peak shear locations of shear segments within a features, and 3) provide for separation of features which is essential for the detection of the radial convergence areas around microbursts and secondary outflows.

Feature error checking begins by searching a feature for consecutive shear segments with the same azimuth. If a pair is found, the peak shear locations (azimuth and range) of both segments are compared to the location of the shear segment preceding the paired segments. The paired segment whose peak shear

range is closest to the peak shear range of the preceding segment remains part of the original feature. The other segment is removed from the original feature and is stored until all shear segments of the feature have been checked by the above procedure. The set of removed shear segments are then examined in an attempt to build new features using the algorithm's original feature building constraints. An example of a feature with segments from the same azimuth is given in Figure 1. The secondary area of radial convergence is highlighted in yellow.

Feature error checking may separate the convergent areas on either side of a microburst into two features as shown conceptually in Figure 2. It may also remove enough shear segments from a feature such that the feature no longer meets the feature building constraints or other algorithm thresholds.

A sample group of 1916 features, from both the FL-2 Denver and Kansas City data bases, were checked using this procedure. In all, 397 features (20.7%) contained at least one pair of consecutive shear segments with the same azimuth. The maximum number of paired segments observed for an individual feature was 51.

Typically, only one or two shear segment pairs (same azimuth) were contained in a feature and feature error checking simply removed one or two segments. This occurred with 250 (13.0%) of the features. Feature error checking completely deleted 42 (2.2%) of the original features. Feature deletions were typically observed

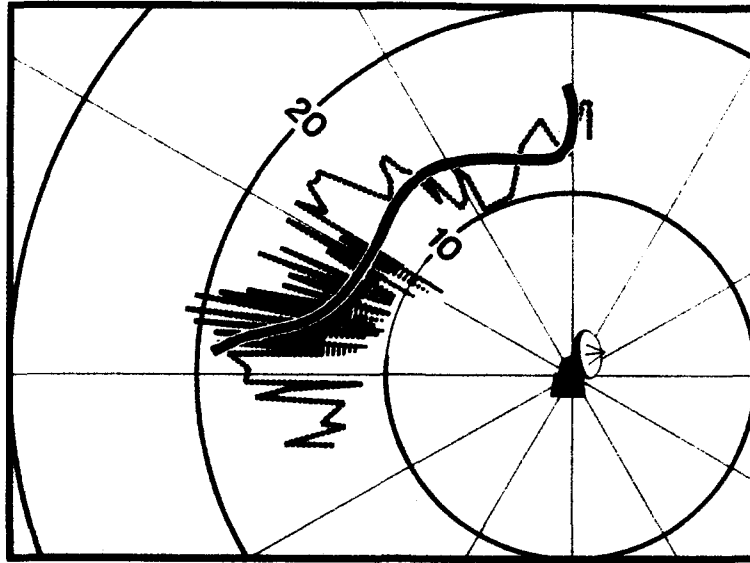


Figure 1. An example of a feature (dashed green) that includes shear segments from the same azimuth. The dashed lines connect the peak shear locations of the individual shear segments. The secondary radially convergent area is highlighted in yellow. The algorithm detection (bold red curve) is improperly positioned in a divergent area.

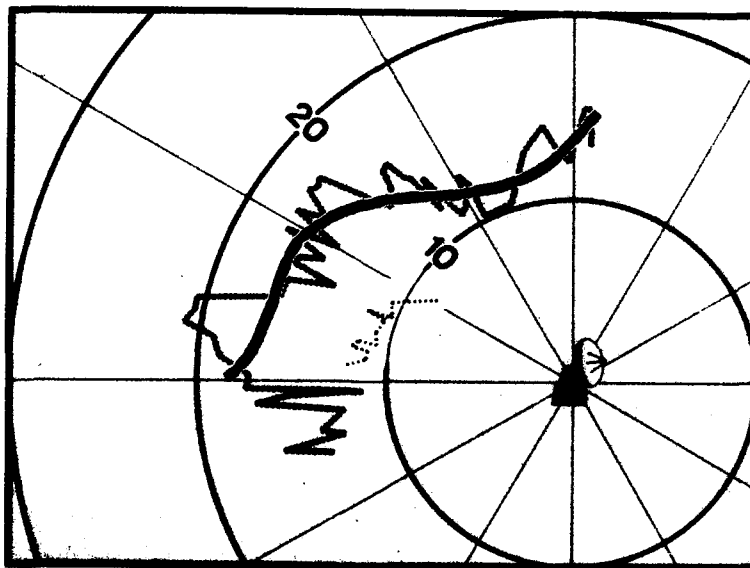


Figure 2. The feature from Figure 1, now two features, after the error checking procedure. Note that the new gust front detection (bold curve) more closely matches the convergent area furthest in range. The secondary convergent area did not pass the front length threshold of 10 km.

in association with the short, clutter and second trip echo induced features that had barely passed the original feature building constraints.

Features error checking split the remaining 105 (5.5%) features into two or more features. This occurred when the segments were either produced by the convergent areas around a microburst, by multiple surges in thunderstorm outflows, or by spurious convergent features near ground clutter regions.

3.B. Vertical Association

In order to reduce the number of false front detections by the gust front algorithm, a vertical association test was added to the algorithm prior to the 1988 TDWR OT&E. To produce a gust front detection, features from the lower elevation scan must be associated with features from the upper elevation scan. In the 1988 TDWR OT&E algorithm, features satisfied the vertical association requirement if the centroid of one feature was within the "vertical continuity box" of a feature from a different elevation scan (Witt et al., 1989). However, vertical association was not required if: a) the longest feature was greater than 15 km in length, and b) the longest feature within 10 km of the radar was detected on the upper level scan (1.0°) and no candidate fronts were within 10 km of the radar. The latter case was to allow for the detection of gust fronts whose 0.5° elevation scan features might be shortened by ground clutter removal close to the radar.

From post analysis, the gust front detections produced by

above conditions, a) and b), were determined to be a primary source of false alarms near the radar. As a result, relaxations of the vertical association criteria near the radar, without additional constraints (i.e, time continuity), is not recommended. However, improvements to the overhead tracking technique (Section 5) should facilitate the detection of many gust fronts passing near the radar.

The vertical continuity box technique, which is a function of a features' length and centroid location, worked well when gust fronts were somewhat straight. However, the technique did not always associate features from curved gust fronts because the centroid of a feature at one elevation might not fall within the vertical continuity box of a feature at the other elevation. An example of features from a curved gust front that were not associated by this technique is given in Figure 3.

Occasionally a centroid of a feature was located in the vertical continuity box of an unrelated feature and generated an incorrect association. Thus, the vertical continuity box technique also allowed for erroneous associations which produced both false alarms and missed detections.

To associate features more appropriately in the vertical, a new technique was implemented. Using a feature at one elevation scan, the distances between each of this feature's end points and all the peak shear locations of a feature on a different elevation scan is computed. If any of the distances are less than or equal

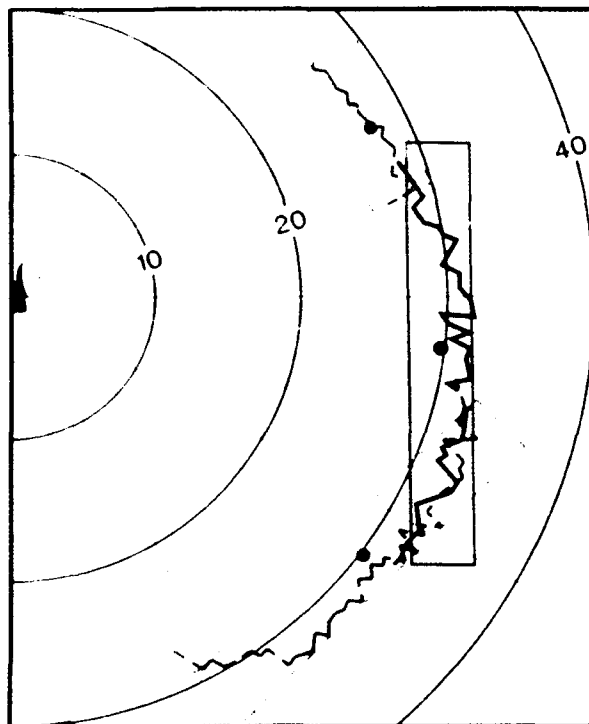


Figure 3. Lower scan features are represented by dashed lines and have dashed vertical continuity boxes. Upper scan features are represented by solid lines and have solid vertical continuity boxes. Feature centroids are represented by (.).

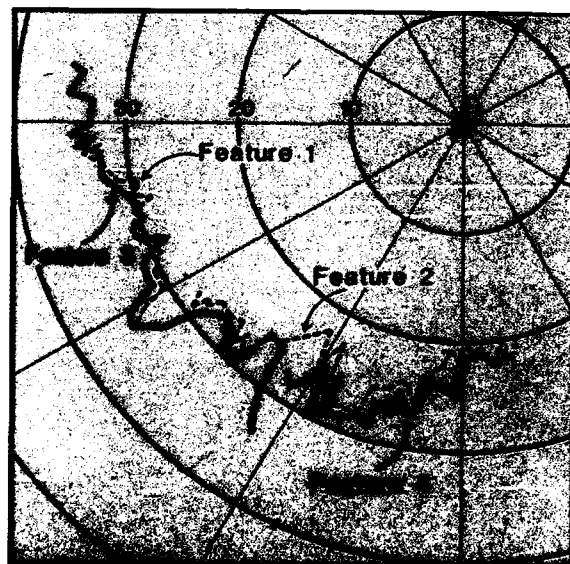


Figure 4. Four features that form a candidate gust front detection. Dashed lines represent features on the lower scan while solid lines represent features on the upper scan. Association is accomplished using the end point comparison technique.

to an adaptive threshold (2 km), vertical association is established and a "scan feature pair" is created. These comparisons are repeated for all combinations of lower and upper scan features. This "end point comparison" technique allows features from with a variety of orientations, overlaps, and curvatures to be vertically associated.

Once vertical association is established, each scan feature pair is entered into a table for subsequent comparison. Figure 4 shows an example of three feature pairs that identify a front. Features 1 and 2 occur at the lower elevation and are represented by the dashed curves, while Features 3 and 4 occur at the upper elevation scan. Feature pairs of [1,3], [2,3], and [2,4] were all entries in the vertical association table. Thus the detected gust front is a composite of Features 1, 2, 3, and 4.

An example of the improvement in the detection of curved gust fronts is given in Figure 5. Statistics to demonstrate the improvement in overall gust front detection using the end point comparison technique are summarized in Table 1. The data base for the statistics covers 13 days and 266 volume scans obtained by the FL-2 radar located in Denver during 1988.

Most notable of these results are the improvements to the detectability of gust fronts, i.e., entries 2, 3, and 4 of Table 1. In addition, any improvements in front detectability and representation produce improvements in both the forecasting of gust fronts and wind estimates.

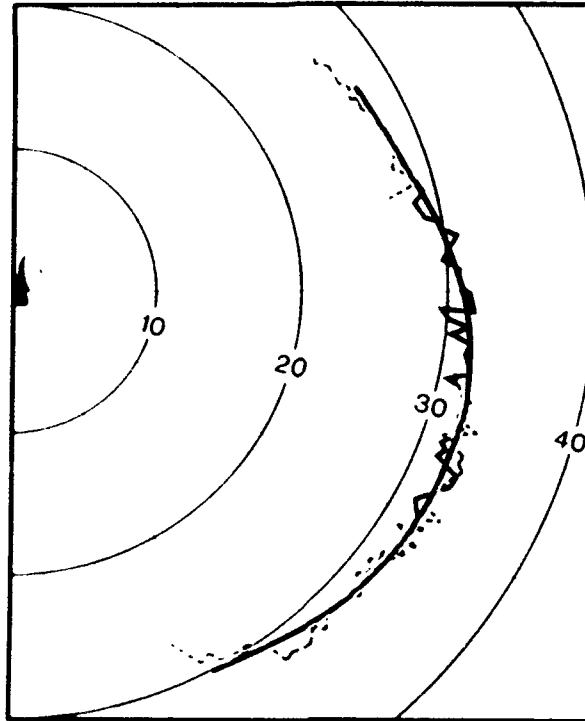


Figure 5. Detection of a curved gust front (bold red curve) produced by vertical association using end point comparisons. These features were previously unassociated using the vertical continuity box (Figure 3). Dashed lines represent features on the lower scan. Solid lines represent features on the upper scan.

Table. 1. Percentage of Gust Front Detections Modified using the End Point Comparison Technique Rather than the Vertical Continuity Box

Fronts that were modified (2 or 3 fronts merged into one front)	9%
Fronts not detected with vertical continuity box, but detected by end point comparison	4%
Fronts lengthened	3%
False alarms eliminated	5%
Failures (misses or minor errors)	1%
Severe failure (1 case in 433)	0.2%

3.C. Detection of Fronts Tracking Over the Radar Site

As a gust front propagates toward the radar, the portion of the front having significant radial convergence (greater than a 5 m s^{-1} velocity difference across the frontal zone) decreases. For a front with a uniform velocity difference of 10 m s^{-1} and length of 50 km, the decrease in algorithm detection capability as a function of radar range is given in Figure 6. For this simple representation, as the radar range decreases from 15 to 5 km, the maximum detectable length (bold curve) decreases to $\sim 10 \text{ km}$. The detection of close-in gust fronts may be even further degraded by non-uniform intensity, different orientations or curvatures, and/or different propagation directions, along with data artifacts produced by ground clutter removal and beam blockage.

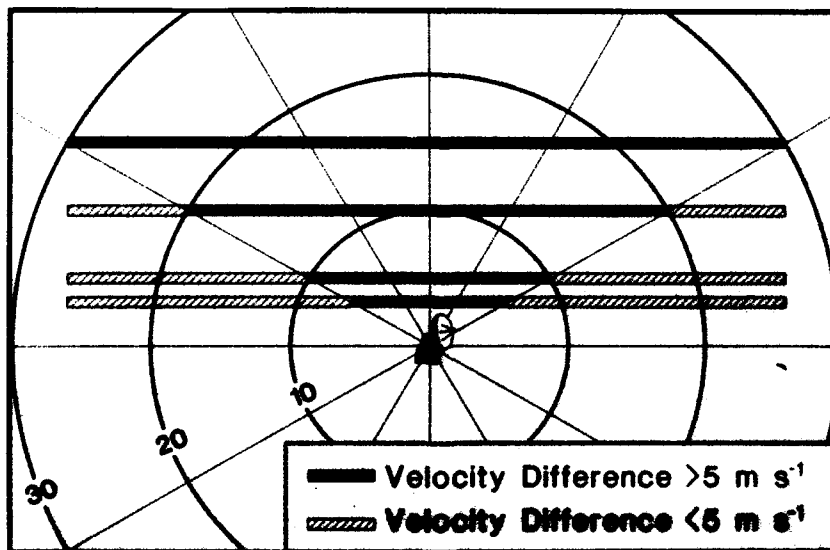


Figure 6. An example of reduced algorithm detection capability for a front with uniform velocity difference (10 m s^{-1} and length (50 km) approaching the radar. The solid curve indicates convergence areas where velocity difference is greater than or equal 5 m s^{-1} . Hatched area indicate a velocity difference of less than 5 m s^{-1} .

Although a method for detecting fronts tracking over the radar was already present in the algorithm, its design did not provide wind estimates, wind shear hazard estimates, or forecasts of future locations. This overhead tracking technique simply used the location of the five-minute forecast generated from the previous volume scan as the detection ("coasting"). Additionally, the design had never been tested during real-time operations. For these reasons, the overhead tracking technique was redesigned.

The objectives of the new technique are to maintain the length and accuracy of front detections as long-lived gust fronts pass over and near the radar. Thus, time continuity constraints, orientation checks, and spatial proximity checks, not previously utilized, are included to help facilitate accurate detections. The following text describes the revised technique.

Overhead tracking is initiated when a gust front's centroid is within an adaptive range threshold (20 km) and it is propagating towards the radar with a speed greater than an adaptive speed threshold (4 m s^{-1}). A front centroid is the average of the x, y locations of the its shear features. In addition, the front must have been detected on the two previous volume scans. This helps to ensure that the front is not a transient phenomenon.

Once a front is chosen to be overhead tracked, special rules are used which try to maintain the detection and its length as it passes over the radar. The algorithm attempts to match the front chosen for overhead tracking with detections from subsequent volume scans. A match is established if the two fronts are time

associated (see Section 2) and the orientation difference between the fronts is less than 45° . If a match is found, the forecasted locations, available at one minute intervals, are examined to see which is the nearest to the current detection. With the goal of maintaining length, the selected forecast is merged with the current detection. A final representation is obtained by smoothing these locations using a polynomial of the appropriate order (third or fifth).

If no time association between the overhead tracked front and a detection from the next scan results, coasting is used to generate a detection. The coasted location is determined by the front's propagation speed, the time difference between scans (approximately 5 minutes), and the location from the previous scan.

The overhead tracking process is aborted if, 1) the overhead tracked front moves outside of the range threshold (20 km), 2) the front's propagation speed decreases to 2 m s^{-1} below the threshold speed, 3) coasting persists for more than 12 consecutive volume scans (site-adaptable threshold), or 4) two fronts are time associated but have orientations that differ by more than 45° .

A sequence of gust front detections (Figure 7) shows how detections are sustained and lengthened by overhead tracking. The detections in Figures 7b, 7c, 7d, and 7e are examples of "coasting". Once overhead tracking is initiated, the wind shear hazard estimates and the wind estimates behind the front, for the current detection, are set to those estimates from the overhead tracked front. If a detection is generated by coasting for more

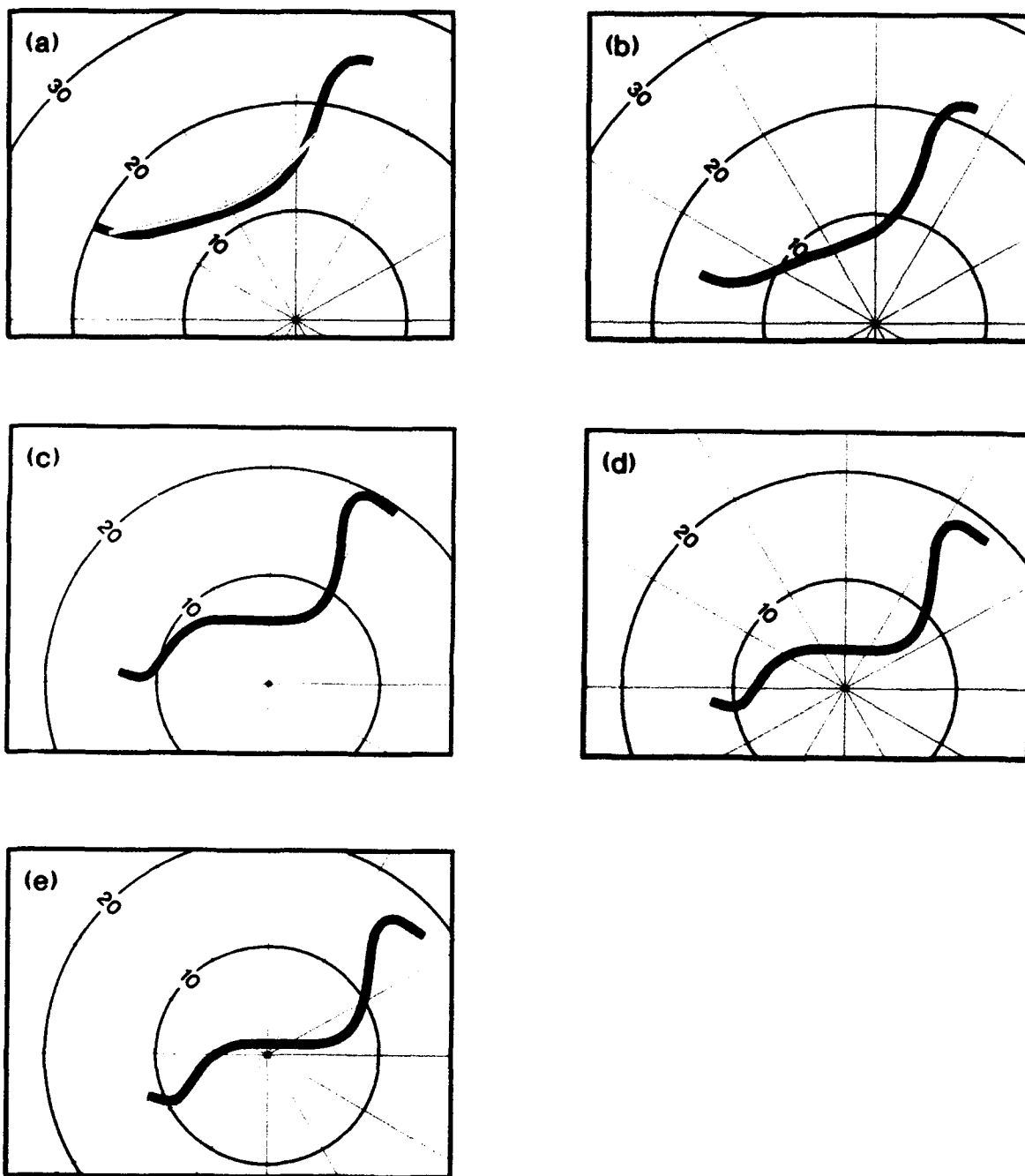


Figure 7. Gust front detections (a-e) for 5 of 9 volume scans at ten minute intervals. The thin cyan curve indicates the detection without the overhead tracking technique. The bold red curve is the detection produced using overhead tracking.

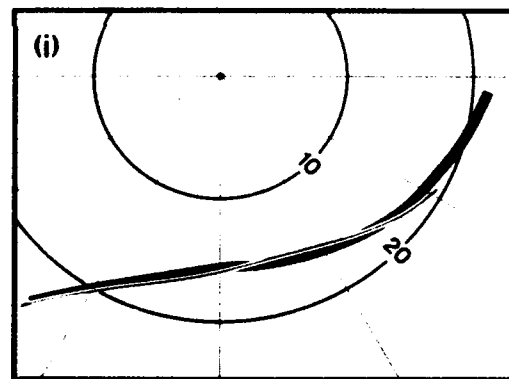
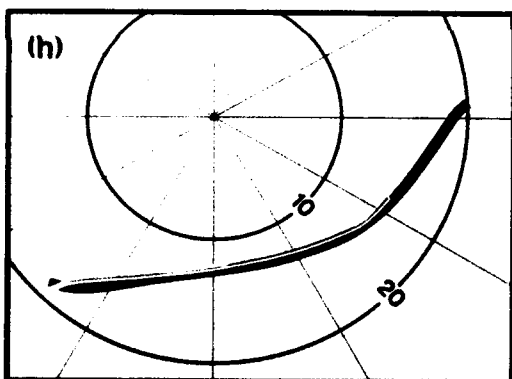
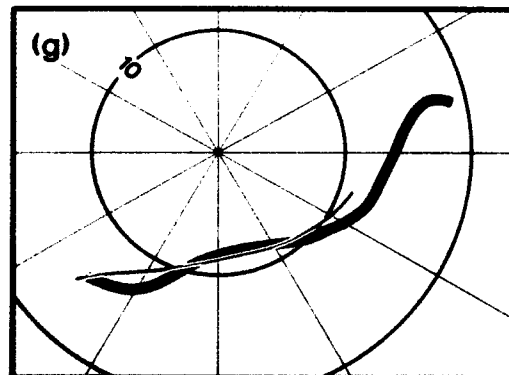
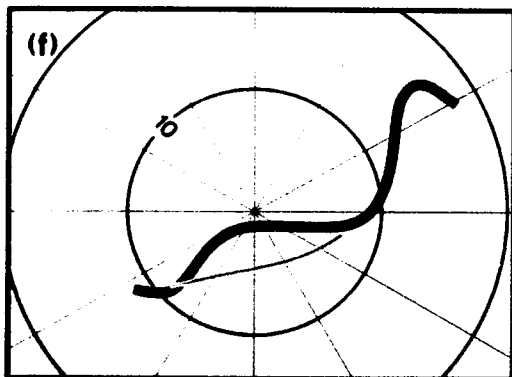


Figure 7. (continued) Gust front detections (f-i) for 4 of 9 volume scans at ten minute intervals. The thin cyan curve is the detection without the overhead tracking technique. The bold red curve is the detection produced using overhead tracking.

than 3 scans, its wind shear hazard estimate is set to zero.

Testing of the new overhead tracking technique was done using FL-2 Doppler radar data collected in Denver (1988) and Kansas City (1989). Data sets with known false detections caused by low-level jets, typically occurring within the overhead tracking range, were included in the data base. A total of 203 scans with fronts passing over or near the radar were processed. The algorithm with overhead tracking detected 176 of 203 of the fronts (97%). Without overhead tracking, the algorithm detected 142 of 203 of the fronts (70%). Because the overhead tracking technique assumes steady-state motion, false detections may be created when gust front propagation speed rapidly increases or decreases over the period of a volume scan. For the 203 scans used for evaluation, the algorithm without overhead tracking produced 18 false alarms. The algorithm with overhead tracking produced 24 false alarms. Thus, a false alarm ratio (FAR, the number of false detections divided by the number of good detections plus false detections) of 12% was maintained. The additional false alarms were not associated with the low-level jet phenomenon, but were associated with gust fronts whose propagation speeds deviated from a steady state assumption.

3.D. Gust Front Orientation

Improvements to the vertical association procedure have brought to light deficiencies in the technique used to estimate the orientation of gust fronts. Proper orientation estimation is essential for an accurate gust front representation because it

determines the alignment of the coordinate system where the polynomial curve fitting is performed. The computed orientation also impacts on the quality of the wind estimates behind gust fronts and propagation directions for fronts.

The 1988 OT&E algorithm used the orientation of the longest feature of the front to represent the gust front orientation. At times this adversely affected the polynomial fitting technique. For example, in Figure 8, the front orientation, as computed by the old method, was parallel to the x-axis. The hatched portions of the associated features have several y values that have similar x values, and the attempt to fit a polynomial equation to these points resulted in a curve offset from the feature locations. Since improvements to the vertical association technique specifically enhanced the detection of curved fronts, the scenario depicted in Figure 8 now occurs more frequently. From this example, it is clear that the orientation of the longest feature may not be representative of the actual gust front orientation.

To provide a better estimate of the gust front orientation, a linear fit to all of the vertically associated feature points (peak shear locations) is made. Because the distribution of feature points might contain an extreme range of y values that have the same or similar x values, the acceptability of the initial linear fit is tested by exchanging the x and y coordinates and repeating the linear fit of the feature points. The resultant orientation angles of the two linear fits are compared. If the linear fit

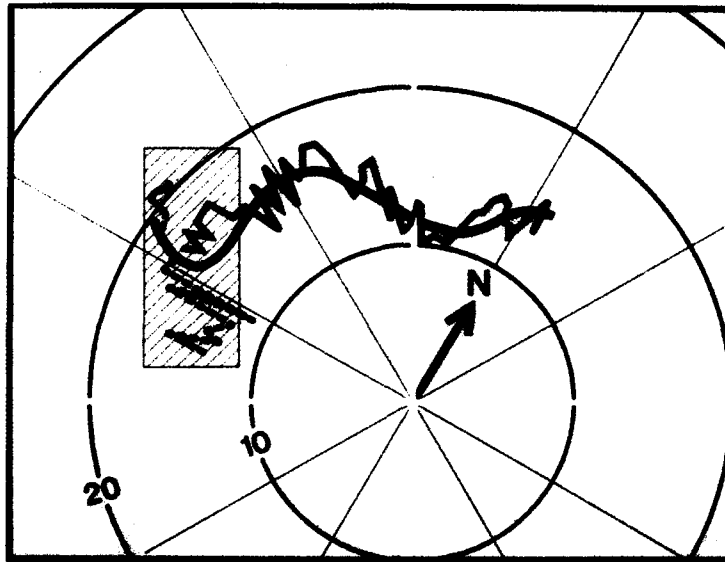


Figure 8. Example of gust front detection (bold curve) when front orientation is set to the orientation of the longest feature prior to polynomial fitting. The hatched region defines a subset of y values that have similar values of x. Dashed lines indicate features from the lower elevation scan. Solid lines indicate features from the upper elevation scan.

provides a good estimate of the orientation, the sum of the two angles will be close to 90° . Testing has shown that if the sum of the angles is greater than 60° , the resultant orientation is satisfactory. If the sum of the two angles is less than 60° , front orientation is determined by the slope of the line perpendicular to a line drawn from the Cartesian coordinate system origin to the front centroid.

Statistics for this new technique were computed for 190 fronts using the 1988 TDWR Denver data base. When the sum of the two orientation angles was 60° or greater, the results showed there were no failures in determining an appropriate front orientation.

Cases where fronts "hook" or "split", such that no single orientation was representative, are discussed in the following section.

3.E. Feature Checking Prior to Polynomial Fitting

Limitations in the polynomial fitting procedure have become evident as a result of improvements in feature detection and association. These are manifested in the detections of fronts that resulted from vertically associated features that contained one or more hooks or splits (Figure 9), i.e., an extreme range of y values for a given x value.

The solution to the polynomial fitting problem involves the identification and removal of a minimum number of feature points so that an accurate representation of the gust front location will be maintained (Figure 10). The procedure to identify and remove feature points is performed in a rotated coordinate system whose x-axis is parallel to the gust front orientation.

To identify a hook or split in the feature points, a check for a large range of y values (> 8 km) over a small interval (1 km) on the x-axis is performed. For each x-axis increment, the difference between the largest and smallest y values is calculated. If this difference is greater than 8 km, and if feature points with both positive and negative y values are within that increment, the points with negative y values are removed, e.g., Areas A1 and A2 in Figure 10. Points within Area B remain because the range of the y values in each x-axis increment is less than 8 km.



Figure 9a. The dashed lines represent features from the low elevation scan and the solid lines represent features from the upper elevation scan. The bold line is the resultant detection after polynomial fitting. "Hook" region is highlighted in yellow.

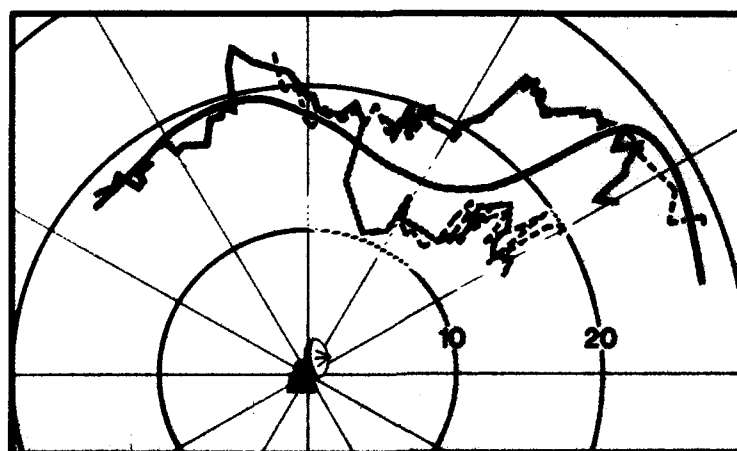


Figure 9b. The dashed lines represent features from the low elevation scan and the solid lines represent features from the upper elevation scan. The bold line is the resultant detection after polynomial fitting. "Split" region is highlighted in yellow.



Figure 10. Example peak shear locations (.) for a front that undergoes point removal by the technique described in this section. Points within Areas A1, A2, and C are removed. Points within Area B remain. The x-axis is parallel to the front orientation. Range rings and north arrow show the radar coordinate system for reference.

In some cases, feature association creates a gap in the feature points, such that additional checking is necessary. If the gap along the x-axis (< 5 km) involves feature points with positive y values, the corresponding points with negative y values are removed. One such gap is found between $x = -10$ and $x = -9$, in Figure 10. Thus, the points in Area C are removed.

On rare occasions, a 1 km x-axis increment may contain feature points whose y values are all positive (or negative) and whose range is greater than 8 km. Feature points whose y values are more than 4 km away from the interval's mean y value are removed.

After point removal, the remaining feature points are then used to produce the polynomial fit to the gust front location. Although the point removal process decreases the percentage of gust front length detected, the front representation remains accurate for a large portion of the fronts with hooks or splits. Sample solutions for the gust fronts in Figure 9 are shown in Figure 11.

This procedure was tested on 232 Denver gust front cases from 1988. The results show that 217 (93.5%) of the gust front detections were not appreciably affected by the removal of feature points (i.e., a change was barely discernable on overlay plots). However, 13 (5.6%) of the gust front detections were changed significantly (e.g., Figure 11). For one gust front, both the original detection and the detection after the point removal procedure were bad representations. Only one detection was slightly degraded from the original detection.



Figure 11a. The front detection after the removal of the hook feature points from the example given in Figure 9a.

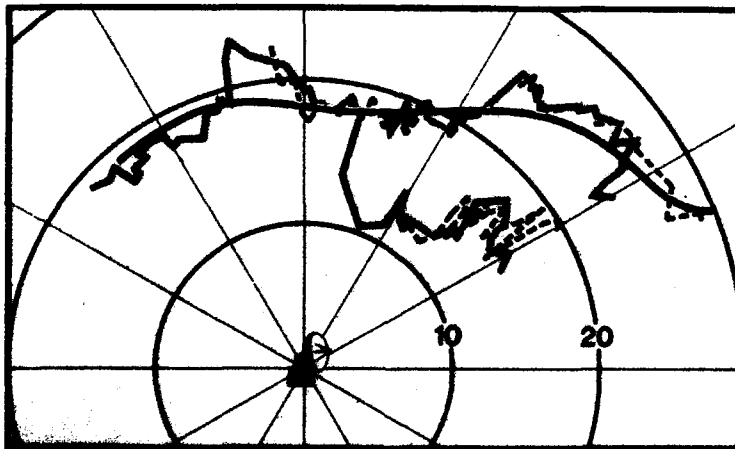


Figure 11b. The front detection after the removal of the split feature points from the example given in Figure 9b.

3.F. Depiction of Long Gust Fronts

During the 1988 TDWR OT&E, the depiction of long gust fronts (> 20 km) was produced by a fifth order polynomial fit of the peak shear locations from the vertically associated features. On occasion, the front depictions had undesirable wiggles near the ends. Although the fifth order polynomial fit was generally accurate, a smoother depiction of the gust front near the end points is more aesthetic and often improves forecasting.

To produce the desired depiction for long fronts, the algorithm was modified so that both a third and fifth order polynomial fit are produced from the original set of feature points. The estimated end points (last 4 km) of the fifth order fit are now replaced with the end points of the third order fit. The merged set of points is then fit using a fifth order polynomial to smooth out small discontinuities that may arise during the merging process. An example of a frontal depiction produced by merging third and fifth order polynomials is given in Figure 12.

3.G. Gust Front Forecasting

Similar to the vertical association technique used in the 1988 OT&E algorithm, the 1988 OT&E gust front forecasting technique relied on centroids to determine the direction and speed of front movement. The gust front centroid is an averaged value of the all the peak shear locations from the vertically associated features. After two fronts were time associated, the gust front propagation

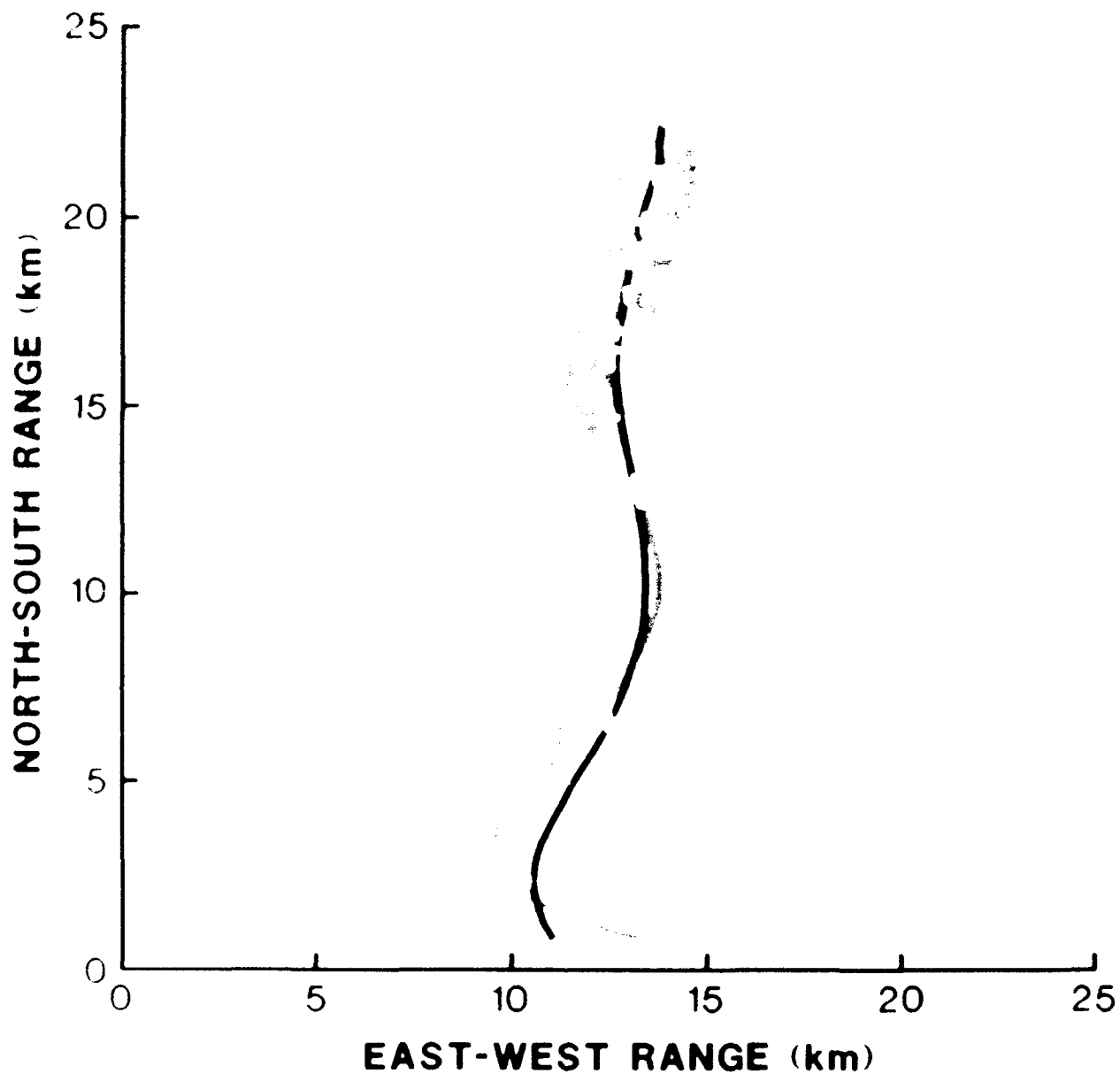


Figure 12. Results from the wiggle fixing procedure. The red curve is an example of a merged third and fifth order polynomial fit. The magenta curve is an example of the original fifth order fit. Square (■) and plus (+) symbols are the peak shear locations of the vertically associated features.

vector was calculated by using the component of the centroid-to-centroid motion that was perpendicular to the line connecting the end points of the gust front from the current volume scan. The gust front propagation vector was then used to translate, at a uniform speed and direction, the points of the current frontal position for each forecasting time interval.

Deficiencies in this forecasting technique relate directly to the use of centroid location calculations, which are heavily dependent on the length and shape of the detected gust fronts. The length and shape of a gust front detection may change considerably from scan to scan. This may simply be caused by a change in the radar viewing angle, but also may be associated with expanding and decaying gust fronts. A gust front may expand like waves produced when a pebble is dropped into a still pond. The waves radiate outward from the source at a uniform speed, but in a direction perpendicular to the wave fronts.

To allow for the forecasts of gust fronts to expand in time, similar to the simple model given above, an improved forecasting technique has been developed. This technique begins by rotating the current detection and the associated detection from the previous volume scan to a coordinate system established by the orientation of the current detection. Front lengths are computed from the polynomial equation utilizing Simpson's Rule (Riddle, 1970). Using the front lengths, arrays of equally spaced grid points (approximately 1 km apart) are obtained for both the previous and current front positions.

From each point on the old front, a perpendicular line is projected onto the current front position. These lines represent the approximate direction that a gust front would propagate based on a model of a radially expanding wave front. Perpendicular lines with lengths greater than two standard deviations from the mean length are removed. This outlier removal procedure is performed twice. If fewer than five "good" perpendicular lines (distances) remain, a forecast is not produced. An example of a front detected at two consecutive scans that fails this test is shown in Figure 13.

All good perpendicular lines (distances) are again averaged and are converted to a mean propagation speed by dividing by the time difference between the current and previous scan. No forecast is made if the value of the propagation speed is extreme ($> 35 \text{ m s}^{-1}$). Forecasts are produced by projecting lines perpendicular to the local front orientation (first derivatives from the polynomial) and in the direction of the average front movement. The frontal position is advanced a distance equal to the mean propagation speed multiplied by the forecasting time interval. An example of a 10 minute forecast, along with the front detected at the time of the forecast, is depicted in Figure 14b. The forecast shown in Figure 14a was produced using the centroid-to-centroid (1988 OT&E algorithm) forecasting technique.

Since the "expansion" method of forecasting may occasionally fail if a portion of a gust front detection is extremely concave, the forecasts are calculated at one minute intervals and a check

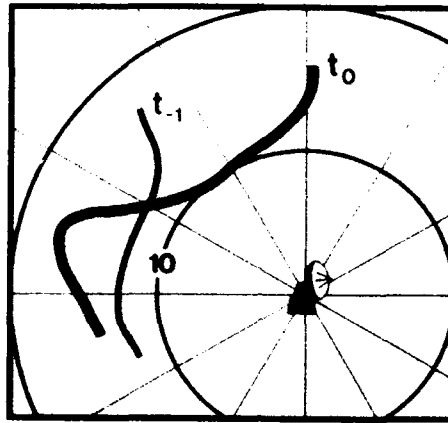


Figure 13. Example of two fronts associated in time (t_0 is the current scan, t_{-1} is the previous scan), for which the forecasting procedure will not produce forecasts.

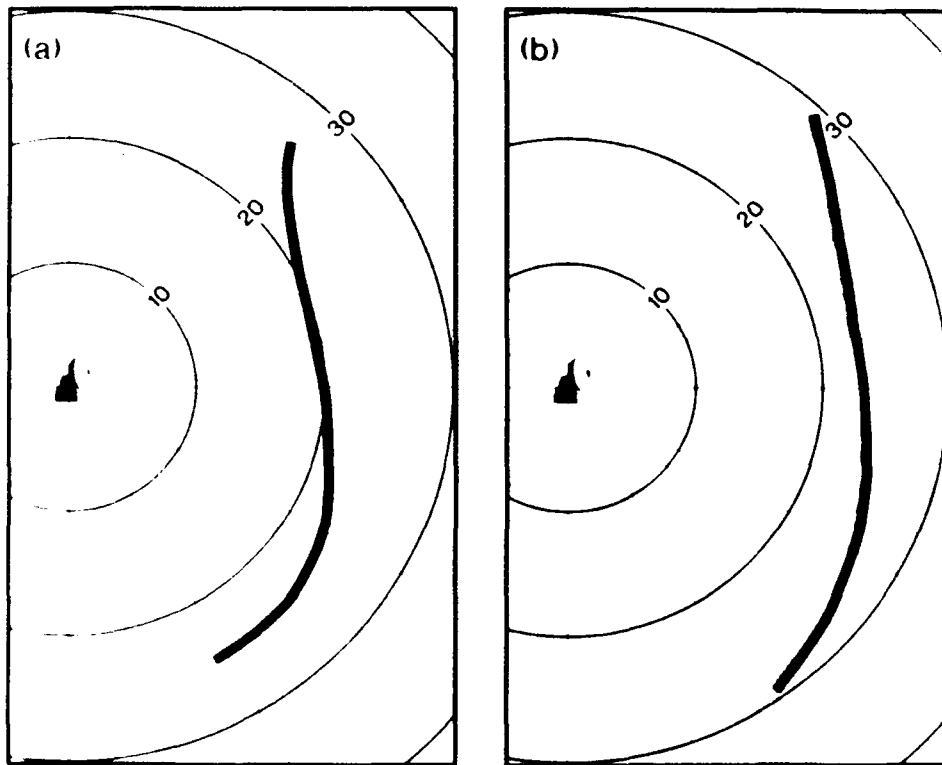


Figure 14. Two examples of 10 minute algorithm forecasts (solid curve), a) using the centroid-to-centroid technique, and b) using the "expansion" technique. The verification front (hatched curve) is provided for reference.

for numerical instability is made. For the cases failing this check, the gust front propagation direction is no longer allowed to vary along the front, rather the direction of motion for all points of the detection is constrained to be perpendicular to the front orientation.

To demonstrate that the improvements to the forecast technique are significant, comparisons were made between 10 minute forecasts, for both the centroid-to-centroid (1988 OT&E version) and expansion forecasts, and fronts detected at the forecast time. Eighty pairs of forecasts and verification fronts, from eight days during 1988 Denver operations, comprised the comparison data base. The mean distances between the 10 minute forecasts and the verification front are categorized in Table 2.

TABLE 2. Distribution of Distances Between Verification Fronts and Forecasts Produce by the Centroid-to-Centroid and Expansion Techniques

Mean Distance Interval (km)	Centroid-to- Centroid Forecasts	Expansion Forecasts
0.0 - 0.5	0	2
0.5 - 1.0	24	29
1.0 - 1.5	17	17
1.5 - 2.0	11	16
2.0 - 3.0	15	11
3.0 - 5.0	10	4
5.0+	3	1

It is observed that both forecasting techniques had peaks in the 0.5 to 1.0 km category of mean distance. However, in the mean distance categories of 2.0 km or greater, the centroid-to-centroid technique had 28 (35%) observations, while the expansion technique had only 16 (20%) observations. Therefore, fifteen percent (12 of 80) of the forecasts showed significant improvement with the new technique. Finally, the overall mean distance between the 80 forecast/verification pairs was 1.92 km for the centroid-to-centroid method and 1.52 km for the expansion technique.

4. False Algorithm Detections Caused by Low-level Jets

Characteristically, the low-level jet is a strong southerly current which is most prevalent in the Spring in the Great Plains during the early evening and nighttime. In many cases, the strong low level winds (20 m s^{-1} and greater) are decoupled from the stable surface layer such that strong vertical shear of horizontal wind may exist in the lowest 2 km of the troposphere. These strong shears may be observed below altitudes of 200 m .

An example of a Doppler velocity pattern produced by a simple model of a jet phenomenon is shown in Figure 15 (Brown and Wood, 1987). The wind direction is uniform with height and the wind speed increases from 0 m s^{-1} at ground level, to a maximum of about 20 m s^{-1} at 4 km, and then decreases to 0 m s^{-1} at 8 km. When the radar beam points westward into the approaching jet, strong

radially convergent shear delineates the jet/stable layer interface. Conversely, when the radar beam points eastward into the departing jet, strong radially divergent shear delineates the interface.

During the operational testing of the TDWR system in the Great Plains (Kansas City), detection of the radially convergent component of the strong shears produced by low-level jets resulted in numerous false detections by the gust front algorithm (e.g. Figure 16). As a result, a study was conducted to determine whether adjustments to algorithm parameters could eliminate these false detections. This involved examination of the algorithm characteristics produced by the low-level jet detections.

From this study, it was determined that the low-level jet detections were a direct result of the detection of convergent radial shear across the jet/stable layer interface. Altering the thresholds used to group shear segments into features had little impact on reducing the number of jet-induced detections. Algorithm thresholds for shear segment attributes of peak shear and velocity difference were given previously in Section 2. Figures 17 and 18 show the distributions of the average peak shear and average velocity difference for 17 jet and 41 gust front detections produced by the algorithm. Here "average" describes an average determined from all the shear segments that make up the detection.

Table 3 gives the mean values of average peak shear and average velocity difference for these same algorithm detections.

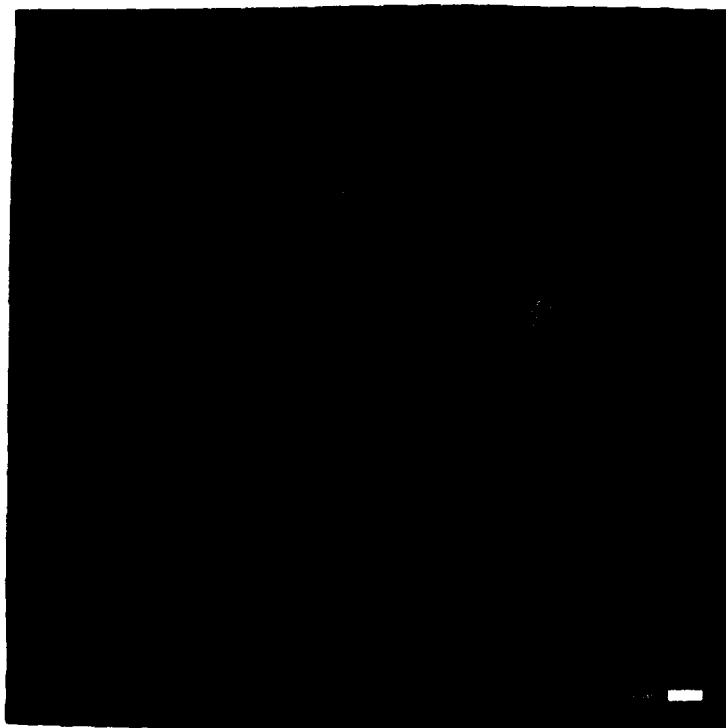
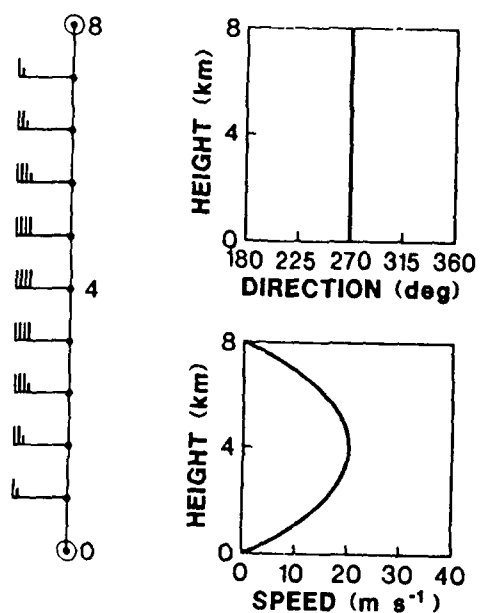


Figure 15. A Doppler velocity pattern produced by a simple model of the jet phenomenon. wind direction is uniform with height. Maximum horizontal wind speed in 20 m s^{-1} .

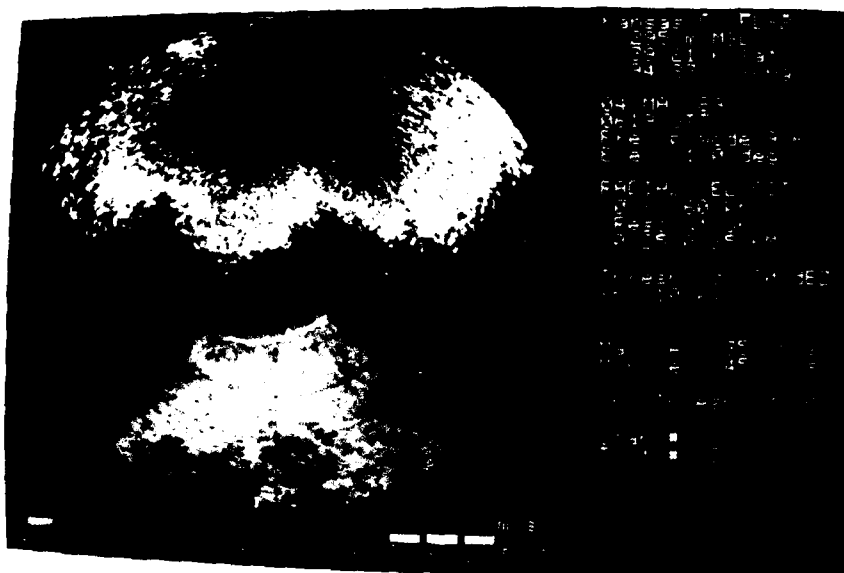


Figure 16. Radar velocity display for May 4, 1989, 0619 UTC from the FL-2 radar's 1.0° elevation scan. The curve is the low level jet detection by the algorithm.

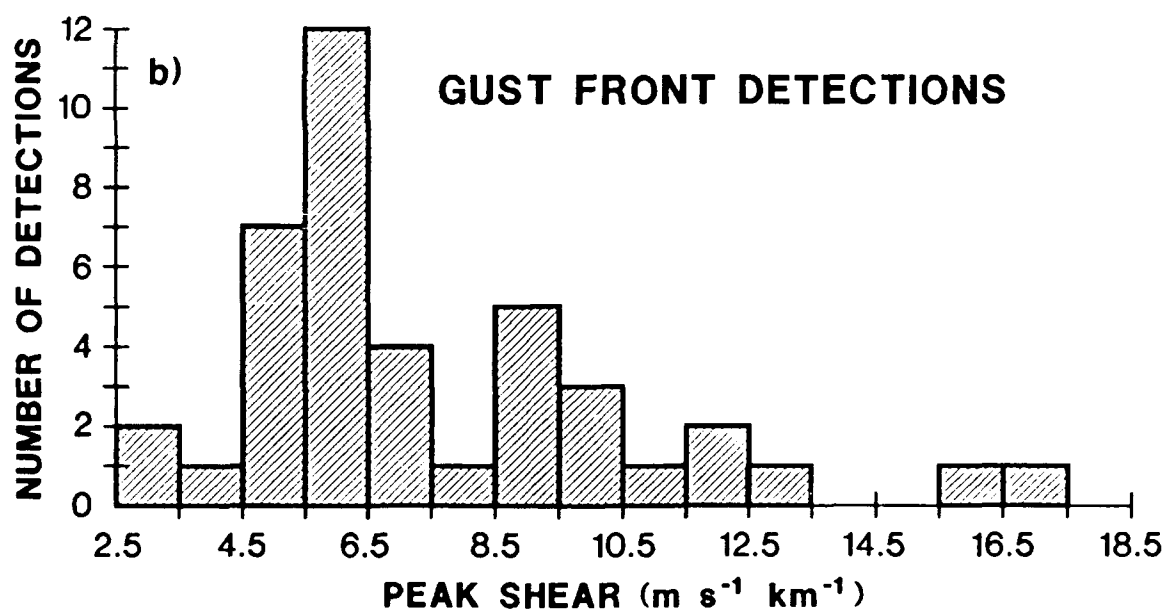
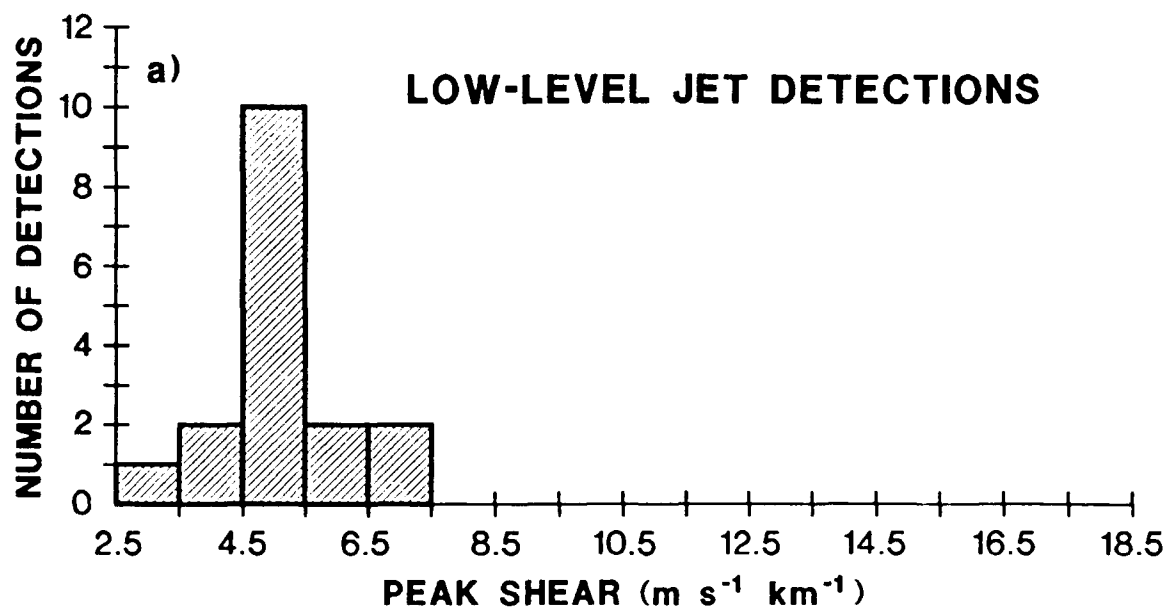


Figure 17. Distribution of average peak shear ($\text{m s}^{-1} \text{ km}^{-1}$) for a) low-level jet detections and b) gust front detections.

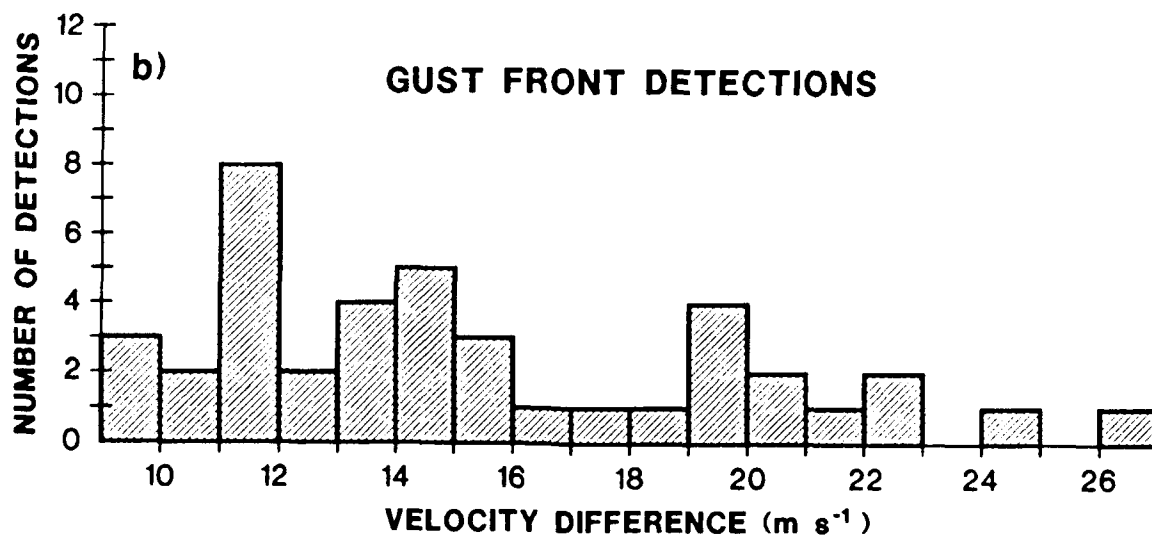
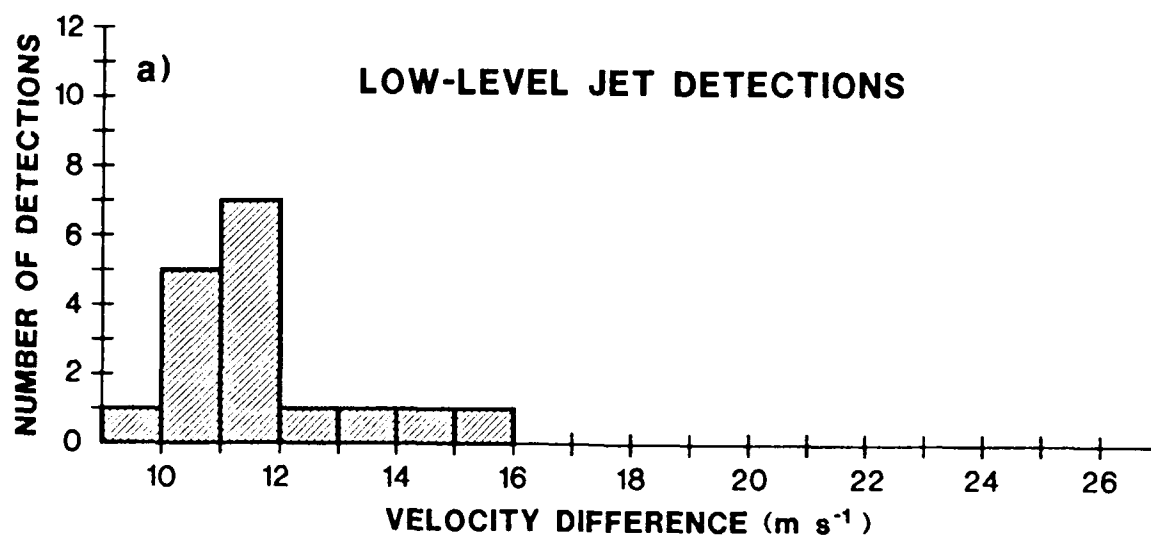


Figure 18. Distribution of average velocity difference (m s^{-1}) for a) low-level jet detections and b) gust front detections.

Table 3 shows that the mean values for both average peak shear and average velocity difference for the 41 gust front detections are somewhat greater than those for 17 jet detections. However, the standard deviation of average peak shear and average velocity difference for the gust front detections are rather large. When the standard deviations are subtracted from the mean values for the gust front cases, the resultant values, for both peak shear and velocity difference, are less than the mean values for the jet cases. Thus, any increase in either shear segment attribute threshold will produce a decrease in both the detection of low-level jet false alarms and gust fronts.

Table 3. Means and Standard Deviations of Average Peak Shear ($\text{m s}^{-1} \text{ km}^{-1}$) and Average Velocity Difference (m s^{-1}) from 41 Gust Fronts and 17 Low-level Jet Detections

Average Peak Shear	Mean	Standard Deviation
Gust Fronts	7.4	3.1
Low-level Jets	5.1	0.9

Average Velocity Difference	Mean	Standard Deviation
Gust Fronts	15.2	4.4
Low-level Jets	11.6	1.6

Since the low-level jet detections have similar algorithm characteristics as weak gust front detections, a change in either the peak shear or velocity difference threshold would result in missed detections of weak gust fronts and portions of gust fronts

where convergent shear is weak, i.e., portions of gust fronts orientated along the radar beam. In addition, the low-level jet detections were typically observed at a distance of 10 to 20 km from the radar. This is the distance that most TDWRs will be sited from the airports. For this reason, it is important to eliminate low-level jet induced false alarms because a large number of the false detections could occur in the airport vicinity. Adjustments to thresholds, that would surely degrade overall algorithm detection capability, do not appear to be the solution to this problem. Rather, input from an algorithm that profiles the winds in the boundary layer (identifying the low-level jet phenomenon), could possibly be used to remove these false alarms.

Although algorithm false alarms may be generated by strong vertical wind shear events such as the low-level jet phenomenon, significant performance gain/loss to aircraft flying through the jet/stable layer interface may occur. A Velocity Azimuth Display (VAD) analysis (Browning and Wexler, 1968) of FL-2 radial velocity data, from elevation scans between 0.3° - 6.5° and from a range of 15 km, depict a low-level jet that occurred on 04 May 1989, near Kansas City, KS (Figures 19 and 20). The low-level jet reached a maximum of 26 m s^{-1} at about 600 m. An aircraft penetrating the low-level jet, on takeoff (6° angle of attack) or descent for landing (3° angle of attack), might experience a performance loss

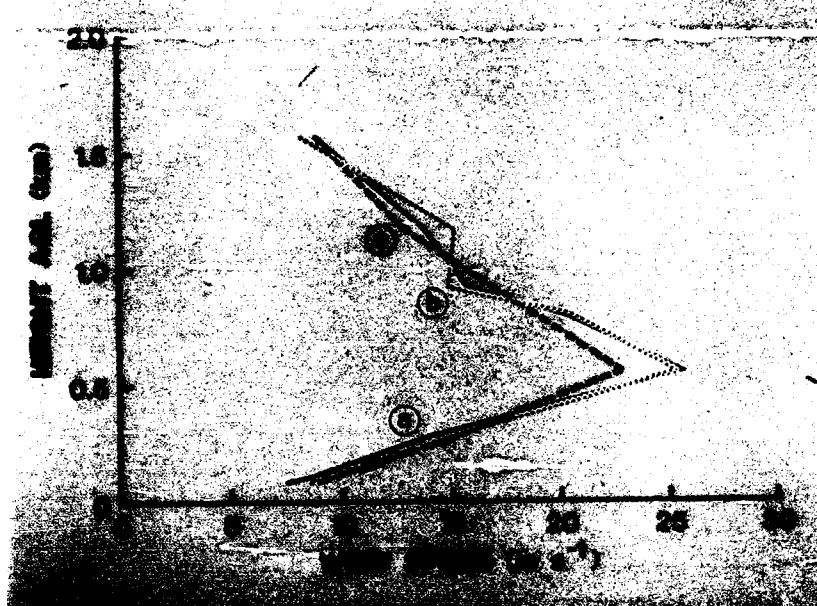


Figure 19. Wind speed versus height for 04 May 1989 low-level jet, for a) 0605 UTC, b) 0621 UTC, and c) 0642 UTC. No surface wind observation was available on this date.

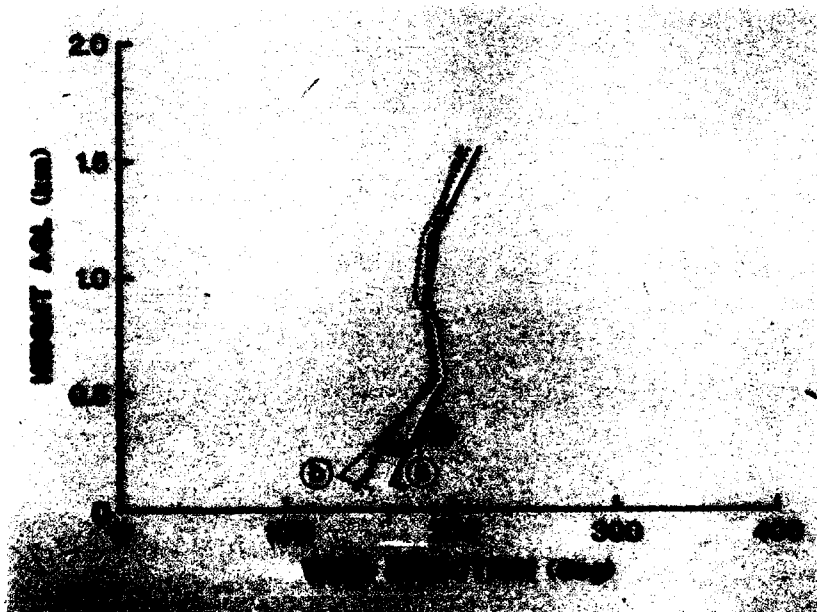


Figure 20. Wind direction versus height for 04 May 1989 low-level jet, for a) 0605 UTC, b) 0621 UTC, and c) 0642 UTC. No surface wind observation was available on this date.

or gain of approximately 40 knots (20 m s^{-1}) (0605 UTC profile) over a distance of about 5 km to 11 km depending on attitude (Lasher, 1989).

5. False Alarm and Wind Estimate Investigations

Although the number of false gust front detections from the Denver, CO data base was low, an investigation into what caused the majority of these cases was conducted. Results showed that the false alarms were either: 1) associated with second trip echo contamination of the radial velocity data, 2) errors in the verification data base, or 3) ground clutter-induced. Two false alarm detections from the Denver data base were produced by high environmental wind speeds similar to the low-level jet phenomenon. Preliminary investigations of algorithm false alarms from the Kansas City data base show that many of these detections were also associated with second trip echoes and additionally, the low-level jet phenomenon.

Problems with the wind estimates behind the gust front detections noticed during the 1988 TDWR OT&E were eliminated by the correction of algorithm coding errors. The data sector, from which the wind estimates were being computed, was significantly offset from the gust front detection whenever the FL-2 radar scanned in a counter-clockwise direction.

6. Conclusions

A thorough examination of the performance deficiencies of the 1988 OT&E version of the gust front algorithm was the motivation for the algorithm enhancements discussed in this report. In summary, these enhancements to the gust front algorithm took several forms: 1) improvement in the detection of curved gust fronts via improvements made in associating features in the vertical, 2) improvement in the detection of fronts passing near the radar using overhead tracking, 3) more accurate detections in the vicinity of microbursts and secondary outflows through the addition of feature error checking, 4) improvement to the wind estimation by correcting a coding error, 5) improvement to gust front forecasts by using the entire length of the current and previous detection to determine front propagation speed, and 6) other enhancements which basically ensure that the algorithm detections are good representations of gust front locations. A good representation of the front's location is vital for proper estimation of both wind estimates and gust front forecasts.

Preliminary performance statistics for the enhanced algorithm were generated using 6 days of the Denver and Kansas City data base (Appendix A). These statistics were generated by comparing algorithm detections with the ground truth locations (represented by a 5 km wide box and subdivided into 1 km bins). Ground truth consists of the gust front location as determined from single Doppler data by experienced radar meteorologists. If any intersection of an algorithm detection and ground truth occurs, the

detection is considered to be a success. The same statistics for the 1988 OT&E version, using the same algorithm thresholds when applicable, were also computed (Appendix A). Using these criteria, the enhancements did not produce a significant change in either the POD or PFA.

After a detailed review of the algorithm performance statistics, it was found that fourteen detections missed by the enhanced algorithm were detected by 1988 OT&E algorithm without vertical association; these detections occurred under the special conditions describe in Section 3.B. All of these detections occurred at ranges greater than 35 km. This suggests that these fronts were shallow and that the upper elevation angle probably overshoot the gust front such that vertical association is not relevant. If the enhanced algorithm is modified to allow for detections without vertical association for this special category of gust fronts, the overall POD and PFA for the algorithm would be 66.6% and 9.4%, respectively. Thus, the enhanced algorithm effectively increased its POD by 3% when compared to the 1988 OT&E algorithm.

Another metric of algorithm of performance is obtained by determining the percentage of the ground truth box length covered by the algorithm detection. The enhanced algorithm provided a slight improvement, 2.2 % increase in percentage of length detected, when compared to 1988 OT&E algorithm (Appendix A). This method of comparing gust front detections against ground truth, however, is not applicable to evaluate the aesthetic appearance of

the detection or the accuracy of the forecasts. It is in these areas that several of the enhancements to the OT&E version have provided significant performance improvements.

Preliminary efforts have begun for the implementation of a new technique to associate front detections in time. The 1988 OT&E algorithm utilizes a centroid-to-centroid comparison to associate gust front detections in time. This is not always reliable for the time association of curved gust fronts. In addition, efforts are being made to improve the number of correct time associations by allowing more than one detection from the current volume scan to be associated with a detection from the previous volume scan. This will allow forecasts to be produced for both parts when a detection splits (decaying front and/or detection problem).

The past success of the gust front algorithm has resulted from an iterative process of algorithm design and substantial testing. With the goal of detecting an even greater percentage of total gust front length, future efforts will concentrate on the integration of azimuthal shear and reflectivity thin line information into the algorithm. In addition, investigations into the types of Doppler radar signatures that delineate smaller scale "ring gust fronts" associated with microbursts are also planned. These continued efforts will ensure that the detailed information available from a single Doppler radar will be used effectively to detect weather hazards to aviation.

7. References

- Brown R.A., and V.T. Wood, 1987: "A guide for interpreting Doppler velocity patterns", NEXRAD Joint System Program Office Report No. R400-DV-101.
- Browning, K.A., and R. Wexler, 1968: A determination of kinematic properties of a wind field using Doppler radar. J. Appl. Meteor., 7, 105-113.
- Klingele-Wilson, D.L., S.H. Olson, W. Wilson, W.P. Mahoney, III, S.D. Smith, A. Witt, and M.D. Eilts, 1989: "Gust front detection algorithm for the Terminal Doppler Weather Radar: Part II: Performance Assessment", 3rd International Conference on the Aviation Weather System, Anaheim, CA, Amer. Meteor. Soc., Boston, MA, 398-402.
- Lasher, S.G., 1989: "A study of two Great Plains low-level jets", Final report for summer study program, National Severe Storms Laboratory, Norman, Ok, 29 pp.
- Riddle, D. 1970: Calculus and Analytic Geometry, Wadsworth Publishing Company, Belmont, CA, 731 pp.
- Smith, S.D., A. Witt, M.D. Eilts, L.G. Hermes, D. Klingele-Wilson, S.H. Olson, and J.P. Sanford, 1989: Gust front detection algorithm for the Terminal Doppler Weather Radar, Part I: Current Status, 3rd International Conference on the Aviation Weather System, Anaheim, CA, Amer. Meteor. Soc., Boston, MA, 31-34.
- Turnbull D., J. McCarthy, J. Evans, and D. Zrnić, 1989: The FAA Terminal Doppler Weather Radar Program, 3rd International Conference on the Aviation Weather System, Anaheim, CA, Amer. Meteor. Soc., Boston, MA, 414-419.
- Uyeda, H., and D.S. Zrnić, 1985: "Automatic detection of gust fronts", FAA Report No. DOT/FAA/PM-85/11.
- Uyeda, H., and D.S. Zrnić, 1986: Automatic detection of gust fronts, J. Atmos. Oceanic Tech., 3, 36-50.
- Witt, A., and S.D. Smith, 1987: "Development and testing of the gust front algorithm", FAA Report No. DOT/FAA/PS-87/4.
- Witt, A., S.D. Smith, M.D. Eilts, L.G. Hermes, and D. Klingele-Wilson, 1989: "Gust front/wind shift detection for the Terminal Doppler Weather Radar", FAA Report (in press).

Appendix A. Algorithm Performance Statistics

Table A.1 Summary of POD and PFA for Enhanced Algorithm

DATE	POD Weak	%	POD Moderate	%	POD Strong	%	POD All	%	PFA	%
06/22/88	32/54	59.3	29/30	96.7	10/10	100.0	71/ 94	75.5	15/ 86	17.4
07/03/88	1/ 5	20.0	16/22	72.7	2/ 2	100.0	19/ 29	65.5	0/ 19	0.0
07/08/88	33/97	34.0	23/25	92.0	7/ 7	100.0	63/129	48.8	7/ 70	10.0
07/10/88	38/53	71.7	38/38	100.0	4/ 4	100.0	80/ 95	84.2	5/ 85	5.9
07/11/88	45/101	44.6	38/55	69.1	18/22	81.8	101/178	56.7	12/113	10.6
08/15/89	15/26	57.7	20/28	71.4	13/16	81.2	48/ 70	68.6	2/ 50	4.0
ALL	164/336	48.8	164/198	82.8	54/61	88.5	382/595	64.2	41/423	9.7

POD = Number of algorithm detections divided by the number of ground truth events.

PFA = Number of false algorithm detections divided by the total number of algorithm detections (true plus false).

Weak = $(5 \text{ m s}^{-1} \leq \Delta V < 10 \text{ m s}^{-1})$

Moderate = $(10 \text{ m s}^{-1} \leq \Delta V < 15 \text{ m s}^{-1})$

Strong = $(15 \text{ m s}^{-1} \leq \Delta V < 25 \text{ m s}^{-1})$

ΔV = Estimate of average peak change in Doppler velocity perpendicular to and along the convergent portion of the gust front.

Table A.2 Summary of POD and PFA for the 1988 OT&E Algorithm

DATE	POD Weak	%	POD Moderate	%	POD Strong	%	POD All	%	PFA	%
06/22/88	32/54	59.3	28/30	93.3	10/10	100.0	70/ 94	74.5	11/ 81	13.6
07/03/88	2/ 5	40.0	12/22	54.5	1/ 2	50.0	15/ 29	51.7	0/ 15	0.0
07/08/88	30/97	30.9	23/25	92.0	7/ 7	100.0	60/129	46.5	6/ 66	9.1
07/10/88	36/53	67.9	37/38	97.4	4/ 4	100.0	77/ 95	81.1	4/ 81	4.9
07/11/88	46/101	45.5	38/55	69.1	19/22	86.4	103/178	57.9	13/116	11.2
08/15/89	16/26	61.5	22/28	78.6	15/16	93.8	53/ 70	75.7	4/ 57	7.0
ALL	162/336	48.2	160/198	80.8	56/61	91.8	378/595	63.6	38/416	9.2

POD = Number of algorithm detections divided by the number of ground truth events.

PFA = Number of false algorithm detections divided by the total number of algorithm detections (true plus false).

Weak = $(5 \text{ m s}^{-1} \leq \Delta V < 10 \text{ m s}^{-1})$

Moderate = $(10 \text{ m s}^{-1} \leq \Delta V < 15 \text{ m s}^{-1})$

Strong = $(15 \text{ m s}^{-1} \leq \Delta V < 25 \text{ m s}^{-1})$

ΔV = Estimate of average peak change in Doppler velocity perpendicular to and along the convergent portion of the gust front.

Table A.3 Average Percentage of Length Detected by the Enhanced Algorithm

DATE	Weak % Length	Moderate % Length	Strong % Length	All % Length
06/22/88	1957.9/32 61.2	1975.8/29 68.1	539.4/10 53.9	4473.1/71 63.0
07/03/88	61.3/ 1 61.3	707.3/16 44.2	86.7/ 2 43.4	855.3/19 45.0
07/08/88	1751.4/33 53.1	1552.8/23 67.5	492.0/ 7 70.3	3796.3/63 60.3
07/10/88	2128.3/38 56.0	2517.2/38 66.2	207.9/ 4 52.0	4853.5/80 60.7
07/11/88	2866.5/45 63.7	2556.6/38 67.3	1198.4/18 66.6	6621.4/101 65.6
08/15/89	943.2/15 62.9	1337.5/20 66.9	842.9/13 64.8	3123.6/48 65.1
ALL	9708.4/164 59.2	10647.2/164 64.9	3367.3/54 62.4	23723.2/382 62.1

% Length = Summation of the percentage of length for the individual detections divided by the number of detections.

Weak = $(5 \text{ m s}^{-1} \leq \Delta V < 10 \text{ m s}^{-1})$
 Moderate = $(10 \text{ m s}^{-1} \leq \Delta V < 15 \text{ m s}^{-1})$
 Strong = $(15 \text{ m s}^{-1} \leq \Delta V < 25 \text{ m s}^{-1})$

ΔV = Estimate of average peak change in Doppler velocity perpendicular to and along the convergent portion of the gust front.

Table A.4 Average Percentage of Length Detected by the 1988 OT&E Algorithm

DATE	Weak % Length	Moderate % Length	Strong % Length	All % Length
06/22/88	1952.7/32 61.0	1867.5/28 66.7	508.3/10 50.8	4328.6/70 61.8
07/03/88	90.4/ 2 45.2	438.7/12 36.6	51.9/ 1 51.9	581.0/15 38.7
07/08/88	1537.3/30 51.2	1497.5/23 65.1	482.7/ 7 69.0	3517.5/60 58.6
07/10/88	1831.8/36 50.9	2352.4/37 63.6	225.1/ 4 56.3	4409.3/77 57.3
07/11/88	2797.7/46 60.8	2610.1/38 68.7	1244.8/19 65.5	6652.6/103 64.6
08/15/89	857.5/16 53.6	1351.4/22 61.4	940.5/15 62.7	3149.4/53 59.4
ALL	9067.4/162 56.0	10117.6/160 63.2	3453.3/56 61.7	22638.4/378 59.9

% Length = Summation of the percentage of length for the individual detections divided by the number of detections.

Weak = $(5 \text{ m s}^{-1} \leq \Delta V < 10 \text{ m s}^{-1})$
 Moderate = $(10 \text{ m s}^{-1} \leq \Delta V < 15 \text{ m s}^{-1})$
 Strong = $(15 \text{ m s}^{-1} \leq \Delta V < 25 \text{ m s}^{-1})$

ΔV = Estimate of average peak change in Doppler velocity perpendicular to and along the convergent portion of the gust front.

Appendix B. Enhanced Algorithm Outline

I. FOR EACH OF THE LOW-LEVEL ELEVATION SCANS

1) For Each Radial

a) Edit Doppler velocities based on

1) Reflectivity threshold (-100 dBZ)

2) Signal-to-noise threshold (0 dB)

b) Dealias velocities, Version 6.0 of NSSL Local Environment Dealiasing

c) Smooth velocities (without reducing data density)

1) If gate spacing < 200 m, 9 gate running average

2) If gate spacing \geq 200 m, 7 gate running average

d) Locate shear segments

1) Find runs (segments) of decreasing velocity in range along a radial

2) Calculate peak shear over 8 gates (6 if gate spacing \geq 200 m)

3) Threshold shear segments based on:

a) Velocity difference between end points of segments

1) 5 m s^{-1} for 0.5° elevation angle*

2) 5 m s^{-1} for 1.0° elevation angle*

* 1) and 2) can be set different

b) Peak shear ($2 \text{ m s}^{-1} \text{ km}^{-1}$)

c) If the velocity difference associated with peak shear is greater than the velocity difference between end points, discard shear segment

- 4) Store important attributes of valid shear segments
 - a) Azimuth
 - b) Range to peak shear
 - c) Peak shear
 - d) Velocity difference between end points
- 2) Build Features
 - a) Shear segments are associated into the same feature if their peak shear locations are within
 - 1) Azimuth threshold (3.3°)
 - 2) Range threshold (2.0 km)
 - b) r, θ peak shear locations are converted to x, y coordinates and are stored in the feature
- 3) Threshold Features
 - a) If number of segments in feature < 5 , discard
 - b) If end point to end point feature length (defined by the locations of peak shear) is < 4 km, discard
- 4) Error Check Features
 - a) If a feature has two shear segments from the same radial, the shear segments of the feature are regrouped into two or more features that are constrained by thresholds a) and b) from the previous section*

* some shear segments are discarded
- 5) Feature Combining
 - a) If the left (right) end point of a feature is within 5 km of the right (left) end point of another feature, the two features are combined
 - b) If end point to end point length of the feature is < 5 km after combination attempt, discard

II. FOR EACH VOLUME SCAN

- 1) Build Fronts by Checking for the Vertical Association of Features from the Two Low-level Tilts
 - a) Compute distances between the end points of one feature and all the peak shear locations of the features from the other tilt
 - b) If at least one distance is ≤ 2 km, store match in table
 - c) Check all possible combinations of lower and upper tilt features
 - 1) Merge features together to form a front
 - 2) If the length of the longest feature of a front is < 10 km, discard the front
- 2) Frontal Depiction, Smooth Locations of Merged Features
 - a) Compute orientation of the front using a linear fit of the merged features
 - b) Compute end point to end point length of the front and centroid location of the front
 - c) Rotate the features into a coordinate system where x-axis is parallel with orientation of the front
 - d) Determine the range of y values within 1 km interval on the x-axis, if range is large (> 8 km), points associated with the negative (positive) y values are discarded if the majority of all y values are positive (negative)
 - e) Fit merged features with high-order polynomial, using segment locations from both low level tilts
 - 1) Third-order polynomial if length ≤ 20 km
 - 2) Fifth-order polynomial if length > 20 km
 - a) Replace outer edges of front approximation, (4 km), with third-order polynomial and refit using fifth-order polynomial
 - f) Rotate front approximation back to original radar x, y coordinate system
 - g) Compute estimate of wind shear hazard

- 1) The average plus one standard deviation of the segment peak shear values from merged features
- h) Write out the front approximation and the wind shear hazard estimate
- 3) If Overhead Tracking Flag was Set During Previous Scan, Overhead Track the Front
 - a) Determine if overhead tracked front associates with a front from the current scan
 - 1) Calculate distance separating the current front midpoint and overhead tracked front midpoint
 - 2) Association established if distance between the centroids is a minimum and is less than the product of 33 m s^{-1} and the time separation between volume scans
 - a) If more than one front is time associated with the overhead tracked front, the overhead tracking flag is cleared
 - b) If the orientation of the associated front is $> 45^\circ$ different than the orientation of the overhead tracked front, the overhead tracking flag is cleared
 - 3) Determine which one minute interval forecast (from previous scan) has the minimum average distance from the midpoint of the associated front
 - 4) Do a polynomial fit of closest forecast and the front to produce a longer detection for the front tracking across the radar
 - b) If no association with a front from current scan, coast the forecast from the previous scan whose time is closest to the time difference between volume scans
 - c) Set the wind shear hazard estimate for the overhead tracked front to the estimate of the associated front from the previous scan
 - 1) If the number of volume scans where the detection is produced by a coast is > 3 , the wind shear hazard number is set to zero

- d) Set the horizontal wind estimate behind the front for the overhead tracked front to the estimate of the associated front from the previous scan
 - e) Write out the front approximation, wind shear hazard estimate, and wind estimate for behind the front
- 4) Time Association of Fronts
- a) Calculate distances separating gust front centroids from consecutive radar scans
 - 1) Time continuity established if distance between two centroids is less than the product of 33 m s^{-1} and the time separation between volume scans
- 5) Forecasting of Fronts Associated in Time
- a) Compute normal distances between previous and current detection every 1 km, and average
 - b) Distances greater than ± 2 standard deviation from the average are rejected; repeat this computation
 - c) Recompute average of the normal distances
 - d) Compute a mean propagation speed
 - e) Produce forecasts by translating points from the current detection
 - 1) A distance equal to the product of the forecast time and the propagation speed
 - 2) In a direction normal to the local orientation of the front
 - 3) Check for forecast stability by checking if x values increase along the front
 - 4) If x values do not increase along the front
 - a) Delete the forecasts
 - b) Produce forecasts by translating points from the current detection
 - 1) A distance equal to the product of the forecast time and the propagation speed

- 2) In a direction normal to the orientation of the gust front
- f) Compute a propagation direction using the midpoints of the current detection and any forecast
- g) If overhead tracking flag is set, store forecasts to use for overhead tracking the front in the subsequent volume scan
- h) Write out forecasts
- 6) Setting or Clearing the Overhead Tracking Flag
 - a) If the flag is not set and was not previously cleared during this volume scan, check if front is within the threshold range (20 km)
 - 1) If front is propagating toward the radar with speed greater than 4 m s^{-1} and if the front has been detected on three consecutive volume scans, set the overhead tracking flag
 - 2) If flag is set, store midpoint location of front to be overhead tracked
 - b) If overhead tracking flag is set, check if overhead tracked front still passes the criteria for overhead tracking
 - 1) If the front has moved outside of the overhead tracking range, clear flag
 - 2) If propagation speed is less than (threshold speed - 2 m s^{-1}), clear flag
 - 3) If the number of coasted detections is greater than the threshold (12), clear flag
 - 4) If flag is still set, update the midpoint location of the overhead tracked front
- 7) Wind Estimates For Fronts Associated In Time
 - a) Define processing sectors, one on each side of the gust front
 - 1) Azimuthal width of sector equals azimuthal extent of gust front, upper limit is 80°
 - 2) Range width of sector is 30 gates (about 4 km)

- 3) Displace sectors 2 km from detected gust front
- b) Fit radar velocity data using a uniform, horizontal wind model
 - 1) Reject data which deviate by more than two root mean squared errors from least-squares fitted values
 - 2) Refit edited radar data to model
- c) Fit radar velocity data using a model that constrains the wind direction to be perpendicular to the front's orientation
 - 1) Reject data which deviate by more than two root mean squared errors from least-squares fitted values
 - 2) Refit edited radar data to model
- d) Determine from tracking information which processing sector is on outflow side (behind) of the front
- e) Select wind estimate
 - 1) If front has $\geq 30^\circ$ extent
 - a) Use uniform, horizontal wind model estimate ahead and behind the front
 - b) Reject estimates behind that are quasi-parallel to gust front orientation
 - c) Reject estimates behind the front if wind direction has a component opposite to front propagation direction
 - d) If estimate behind fails error checks b) or c), replace with the perpendicular model estimate for behind the front
 - 2) If front has $< 30^\circ$ extent
 - a) Use perpendicular model estimate behind the front
 - b) No estimate given for ahead of front
- f) Write out wind estimate behind the gust fronts
- 8) Store Information About Fronts from Current Scan